Available online at www.sciencedirect.com
ScienceDirect
Journal of Crystal Growth 303 (2007) 100–104
JOURNAL OF CRYSTAL GROWTH
www.elsevier.com/locate/jcrysgro

A cellular automata algorithm for step dynamics in continuum modeling of epitaxial growth

Rainer Backofen[a,*], Axel Voigt[a,b]

[a]Crystal Growth Group, Research Center caesar, Ludwig-Erhard-Allee 2, 53175 Bonn, Germany
[b]Institut für Wissenschaftliches Rechnen, Technische Universität Dresden, 01062 Dresden, Germany

Available online 16 January 2007

Abstract

We adapt a cellular automata algorithm in order to track the steps in a continuum model of epitaxial growth and couple it to adatom diffusion at the terraces. The model is capable to treat the Ehrlich–Schwoebel barrier at steps, which leads to instabilities during epitaxial growth. In order to examine the mound formation a nucleation model beyond the mean field approximation is included in our simulations. We show that the meander instability as well as the onset of mound formation can be treated by this model.

Keywords: A1. Growth models; A1. Morphological instability; A3. Ehrlich–Schwoebel effect; A3. Epitaxial growth

1. Introduction

Modeling of epitaxial growth involves the interplay of different length and time scales. In order to predict macroscopic properties of a thin film, information of the atomic processes on the surface has to be transferred to a coarse level to connect atomic length and time scales to macroscopic one. One possibility to treat phenomena of long time and length scale in epitaxial growth is done by continuum models. Here the atomistic processes are modeled by mean field approximation in lateral direction and discrete in height. This has been introduced by Burton, Cabrera and Frank (BCF) in 1951 [1]. The BCF model including the Ehrlich–Schwoebel barrier (ESB) [2] is defined by the diffusion equation for adatom density ρ on the terraces,

$$\partial_t \rho = D\Delta\rho + F - \tau^{-1}\rho, \tag{1}$$

and the kinetic boundary condition at a step from below (+) and above (−)

$$\pm D\left.\frac{\partial\rho}{\partial n}\right|_{\pm} = k^{\pm}(\rho^{\pm} - \rho^{*}(1+\xi\kappa)). \tag{2}$$

$k^{\pm}$ are the attachment rates from below and above and account for the ESB. τ is the desorption rate, ρ^* is the equilibrium density of adatoms at a step, ξ is the step stiffness and F is the deposition flux. The normal velocity v of steps is then defined by mass conservation:

$$v = D\left(\frac{\partial\rho^{+}}{\partial v} - \frac{\partial\rho^{-}}{\partial v}\right). \tag{3}$$

There are several methods published to treat this set of equations which differs in the treatment of the free interface: parametric elements [3], level set [4] and phase field [5,6]. Level set and phase field are naturally capable to treat morphological changes while the strength of parametric elements is the very efficient treatment of effects along the step. We adapt a cellular automata (CA) algorithm to this problem of phase tracking and couple it to the BCF Eqs. (1)–(3). The CA algorithm already proved its capability to treat problems with a lot of free interfaces efficiently [7]. Topological changes and local events as nucleation may be incooperated in a natural way. The intrinsic anisotropy of the CA algorithm is a promising feature of the method to treat anisotropic growth laws in epitaxy.

The paper is organized in the following way. In the first part of the second chapter a finite difference (FD) scheme is shown to solve adatom diffusion, Eq. (1), with the

*Corresponding author. Tel.: +49 228 9656 191; fax: +49 228 9656 187.
E-mail address: rainer.backofen@caesar.de (R. Backofen).

0022-0248/$ - see front matter © 2007 Elsevier B.V. All rights reserved.
doi:10.1016/j.jcrysgro.2006.11.336

appropriate boundary condition. The non-trivial boundary condition, Eq. (2), requires a modification of the method proposed in Ref. [4].

In the second part of the second chapter a new CA algorithm is sketched to treat the step evolution. In the second chapter the method is validated by two typical setups and instabilities in epitaxy: meander instability and mound forming. To simulate the formation of mounds a nucleation beyond the mean field approximation is included in the model [8,9].

2. Method

2.1. Adatom diffusion—finite differences (FDs)

Assuming a given step, the partial differential equation for adatom density with appropriate boundary conditions has to be solved, Eqs. (1)–(3). For thermodynamic boundary conditions a FDs method is presented in Ref. [4]. In order to treat the kinetic boundary conditions, Eq. (2), at the step, the ghost value method used in Ref. [4] has to be extended.

The standard stencil for FD discretization is

$$\Delta\rho_{i,j} \approx \frac{1}{h^2}(\rho_{i+1,j} + \rho_{i,j+1} + \rho_{i-1,j} + \rho_{i,j-1} - 4\,\rho_{i,j}). \tag{4}$$

In the vicinity of an inner boundary, Fig. 1, some of the neighbours of $\rho_{i,j}$ are on the other side of the boundary. They are replaced by ghost values, ρ_x^{G} and ρ_y^{G}, respectively. The ghost values are calculated in order to fulfill the appropriate boundary condition.

The discrete form of the boundary condition, Eq. (2), projected on the x-direction is

$$j_x = -n_x k(\rho(\Theta_x) - \rho^*) = \frac{1}{h}(\rho_x^{\mathrm{G}} - \rho_i), \tag{5}$$

where n_x is the x-component of $\vec{n}$. Superscripts $\pm$ and curvature are skipped in the derivation without loss of generality. A simple linear interpolation of ρ along the intersection of node (i,j) and $(i+1,j)$, Fig. 1,

$$\rho(\Theta) = (\rho_x^{\mathrm{G}} - \rho_{i,j})\Theta + \rho_{i,j}, \tag{6}$$

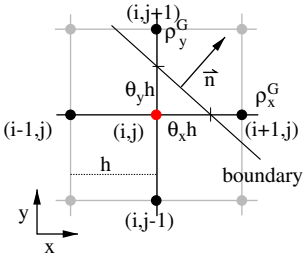

Fig. 1. Sketch of a part of the grid for finite differencing. The grid spacing is h. An inner boundary (step) crosses the grid at two points near node (i,j). $\vec{n}$ is the unit normal to the boundary. The discretization including the treatment of the boundary is described in the text.

leads to an expression for ρ_x^{G}:

$$\rho_x^{\mathrm{G}} = \left(1 - \frac{hk}{1+\Theta_x hk}\right)\rho_{i,j} + \frac{hk}{1+\Theta_x hk}\rho^*. \tag{7}$$

So ρ_x^{G} depends only on nodes on one side of the boundary.

Then the FD stencil for the Laplacian adjacent to a boundary is

$$\Delta\rho_{i,j} \approx \frac{1}{h^2}\left(\rho_{i-1,j} + \rho_{i,j-1} - \left(2 + \frac{hk}{1+\Theta_x hk} + \frac{hk}{1+\Theta_y hk}\right)\right) + \frac{1}{h}\left(\frac{k}{1+\Theta_x hk} + \frac{k}{1+\Theta_y hk}\right)\rho^*. \tag{8}$$

This discretization is used for the Laplacian of nodes adjacent to the boundary and standard FDs are used otherwise. The discrete system is solved using the iterative methods library IML++ [10]. The implementation is tested for various analytical tractable situations, e.g., Fig. 2.

The step velocity is defined by Eq. (3) and can be calculated straightforward [4].

2.2. Step evolution—cellular automat (CA)

Let us sketch the idea of the CA algorithm for the simplest case of a single step. The CA consists of a regular grid of cells. Every cell is in a state, which specifies if this cell belongs to a upper terrace, a boundary or a lower terrace. This already gives a rough description of the morphology of the problem, see Fig. 3. In the CA algorithm the step is more precisely defined by the union of evolution elements (EEs) at the boundary cells. An EE is a rectangle defined relatively to the center of the cell by a set of normals $\vec{n}_i$ and facets f_i, Fig. 3. The union of the EE at the boundary provides a refined representation of the step compared to the CA cells. But to solve for adatom density on the same scale as the CA grid a smoother description of the step is needed. Hence, for every EE tangents $\vec{t}$ to neighboring EEs are constructed. These tangents $\vec{t}$ are used to define a signed distance to the step

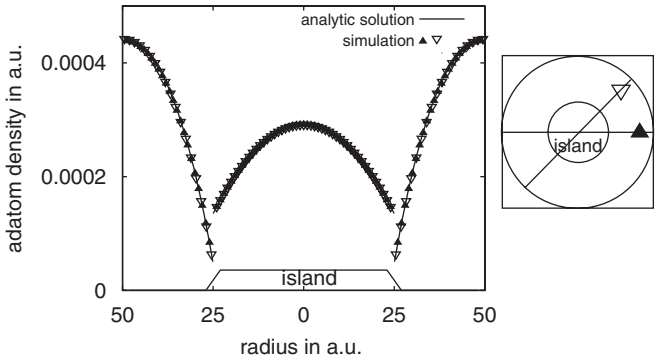

Fig. 2. Stationary adatom distribution for a circular island in the center of a circular region. Boundary conditions at the step are according to Eq. (2) and zero flux at the boundary of the region. Parameters are $(F, D, \rho^*, k_+, k_-, \xi) = (1, 10^5, 10^6, 10^6, 10^5, 0)$. The open and closed symbols indicate different cutting through the two-dimensional adatom field.

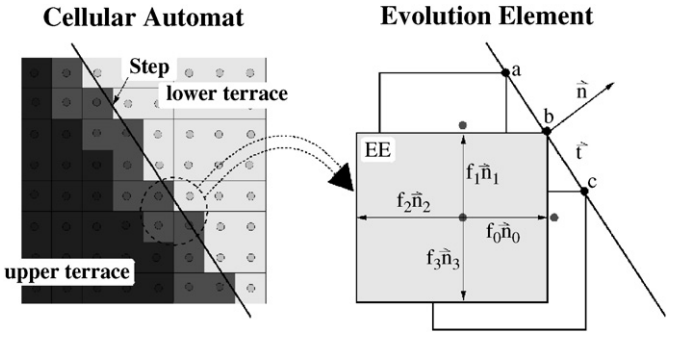

Fig. 3. CA definitions. Boundary cells (dark gray), upper terrace cells (black) and lower terrace cells (gray). The step is represented by tangents $\vec{t}$ to the evolution elements at the boundary cells. That is, the line segments defined by corners a and b (b and c resp.).

for all cells in the neighborhood and the normal to the step $\vec{n}$. The zero isoline of this function is a smooth description of the step and is used to solve the BCF Eqs. (1)–(3).

In order to control the intrinsic anisotropy of the EE the evolution algorithm provided in Ref. [7] has been altered. By solving BCF Eqs. (1)–(3) a normal velocity v is defined in every boundary cell and its vicinity. The evolution algorithm is constructed to propagate a corner of the EE parallel to v, i.e.,

$$f_i \to f_i + \max(v\delta t \cos(\alpha_i), 0), \tag{9}$$

where $\cos(\alpha_i) = \vec{n}\vec{n}_i$ and δt is a time step.

A cell that is a lower terrace is captured by an adjacent EE if its center is inside of the EE. These newly infected cell becomes a boundary cell. Furthermore, a new EE is constructed to represent the step relative to this cell center. Boundary cells surrounded only by boundary or upper terrace cells become upper terrace cells. So the representation and evolution of the step is locally defined by the boundary cells and their neighborhood.

This CA algorithm controls the intrinsic anisotropy given by the EE, Fig. 4. The anisotropy was specially introduced in Ref. [7] to account for the anisotropy in the dendritic structure of a grain. In further studies we want to exploit the anisotropy of the EE to treat anisotropic growth of steps in the BCF framework. But in order to adapt for different anisotropies, e.g., crystal structure, the isotropic case has to be tractable.

The overall algorithm works as follows. The diffusion equation (1) is solved in every timestep by FDs on the grid defined by the CA. The velocity is extracted from the adatom diffusion field according to Eq. (3). This velocity is then used to evolve the step with the CA by Eq. (9).

3. Results

Simulations are done for two configurations: a periodic step train and island growth with nucleation, Fig. 5. If not stated otherwise the used parameters are $(F, D, \rho^*, k_+, k_-, \xi) = (1, 10^5, 10^6, 10^6, 10^6, 0)$ [4,11]. The units are per lattice constant.

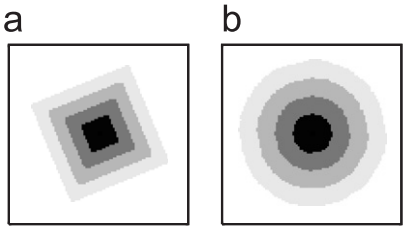

Fig. 4. Simulation of island growth with constant velocity. The gray scale of the islands indicates the growth time. (a) The CA described in Ref. [7] is used. Corners of the EE propagate with constant velocity. The nucleus becomes a rectangular island with the same orientation as the EE. (b) The new CA algorithm is used. The initial nucleus becomes a circular island independent on the EE.

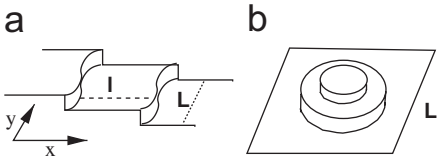

Fig. 5. Setup for simulation of (a) a step train and (b) mound formation. The simulation domain is (a) 100×100 and (b) 80×80 in atomic units.

3.1. Step train

In order to validate the implementation of our method a periodic step train with terrace width l is considered, Fig. 5(a). An ESB leads to the well known Bales–Zangwill (BZ) instability of steps [12,13]. This is a quite interesting feature in epitaxial growth, as this instability may lead to step meandering, which affects the roughness of the surface. In the linear regime the BZ instability is solved analytically [12,13]. Using the same nomenclature as in Ref. [13] and taking the limit of vanishing step stiffness and desorption, the dispersion relation ω is

$$\omega(q, \phi) = \Omega F(d_+ - d_-)\frac{N(q, \phi)}{D(q)} \tag{10}$$

with

$$N(q, \phi) = q(d_+ + d_-)[\cos(\phi) + ql\sinh(ql) - \cosh(ql)] + \tfrac{1}{2}q^2l^2\sinh(ql) \tag{11}$$

and

$$D(q) = [(d_+ + d_-) + l] \times [(d_+ + d_-)q\cosh(ql) + (d_+d_-q^2 + 1)\sinh(ql)], \tag{12}$$

where ϕ is the phase shift between steps, Ω is the atomic area and q is the wavenumber of the perturbation. A measure of the ESB is defined by $d_\pm = D/k_\pm$.

In the limit of vanishing step stiffness there is no most unstable wavelength selected by the BZ instability. To validate the numerics a straight step is initially distorted by a fixed wavelength with a small amplitude.

To investigate a periodic step train with zero phase shift and terrace width $l = 100$ it is sufficient to consider a single step in a periodic domain of length $L = l = 100$.

Fig. 6 shows the logarithm of the amplitude of the step over time for different discretizations. For small times the amplitude increases exponentially. After a while, dependent on discretization the amplitude grows faster. Numerically induced noise is amplified and smaller wavelengths begin to dominate the step evolution. So ω has to be measured as the slope of the logarithm of amplitudes in the linear regime.

As a second validation, the dependence of ω on the strength of the ESB is analyzed in Fig. 7. In the limit of vanishing ESB, $d_+ = d_- = 1$, there is no instability expected and ω tends to zero. As the ESB increases the instability becomes stronger. This is quantitatively well reproduced by our simulation model, Fig. 7.

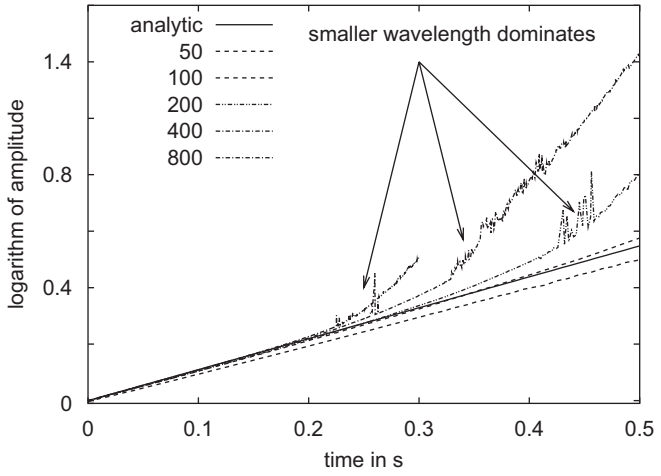

Fig. 6. Logarithm of amplitude over time for various discretizations, labeled by the number of grid points along the step.

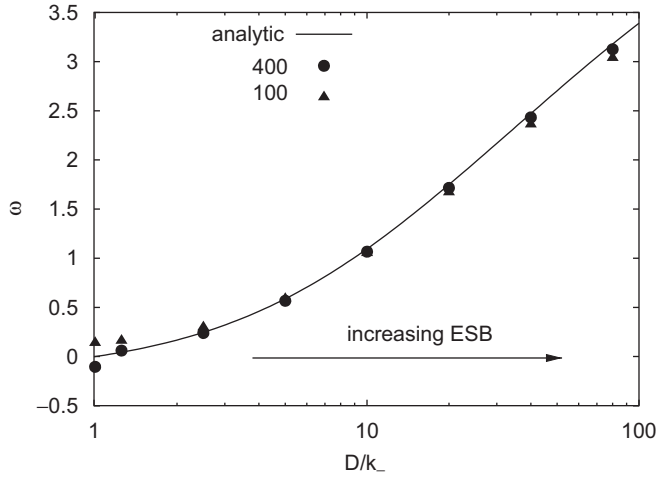

Fig. 7. Dependence of dispersion ω on strength of Ehrlich–Schwoebel barrier (ESB) and discretization. Keeping all other variables fixed D/k_- is a measure for the ESB strength.

3.2. Onset of mound formation

In addition to the BZ instability the ESB may cause a second instability in epitaxial growth: forming of mounds [14]. The nucleation on top of islands is enhanced by the ESB and the impingement of steps slowed down. Both effects may lead to an increase of surface width. In order to model this effects an appropriate nucleation model has to be added to the BCF model.

In the BCF framework, Eqs. (1)–(3), nucleation is the sudden appearance of a new island. So a nucleation model has to define the nucleation rate and the position of nucleation.

Following the work of Politi and Castellano [8,9], the nucleation rate is

$$\omega_{\text{nuc}} = FAW \frac{\tau_{\text{res}}}{\tau_{\text{res}} + \tau_{\text{dep}}}, \tag{13}$$

where the deposition time $\tau_{\text{dep}} = 1/FA$ is the mean time between two deposition events on the island of area A. τ_{res} is the mean residence time of an adatom on an island before attaching to a step. W describes the probability that two adatoms on an island meet before one of them leaves the island. The meeting probability W and residence time τ_{res} are dependent on the strength of ESB as well as the size and geometry of the island [9]. Here we use a model for circular islands on (1 0 0) surfaces with W and τ_{res} defined in Ref. [9].

The probability that no nucleation has occurred up to time t [14],

$$P(t) = \mathrm{e}^{-\int_0^t \omega_{\text{nuc}}\,\mathrm{d}t}, \tag{14}$$

is integrated during simulation. The nucleation position is chosen to be at the position of the maximum adatom density on the island. Thus, nucleation occurs at the center of the island.

First simulations are done with a single island in the center of a periodic domain of size $L = 80$. During growth a new island of fixed small size is put to the top island, whenever the integration of P reaches 0.5 [14]. The surface width over time for different strengths of ESB is shown in Fig. 8(a). Except for vanishing ESB, the surface width is increasing in time. For no ESB the surface begins to grow with a constant surface width after a few layers. An ESB leads to a mound instability, i.e., an increasing surface width. In Fig. 8(b) and (c) the configuration of the steps after 16 s of deposition is shown in case of vanishing and strong ESB. The ESB leads to a mound consisting of about 10 layers. The influence of non-rotational setup is enlarged by the BZ instability and leads to fourfold symmetry. Furthermore, wavy steps occur.

In Fig. 9 the simulations of four regularly arranged mounds are shown. In between the islands deep valleys occur caused by step bunches.

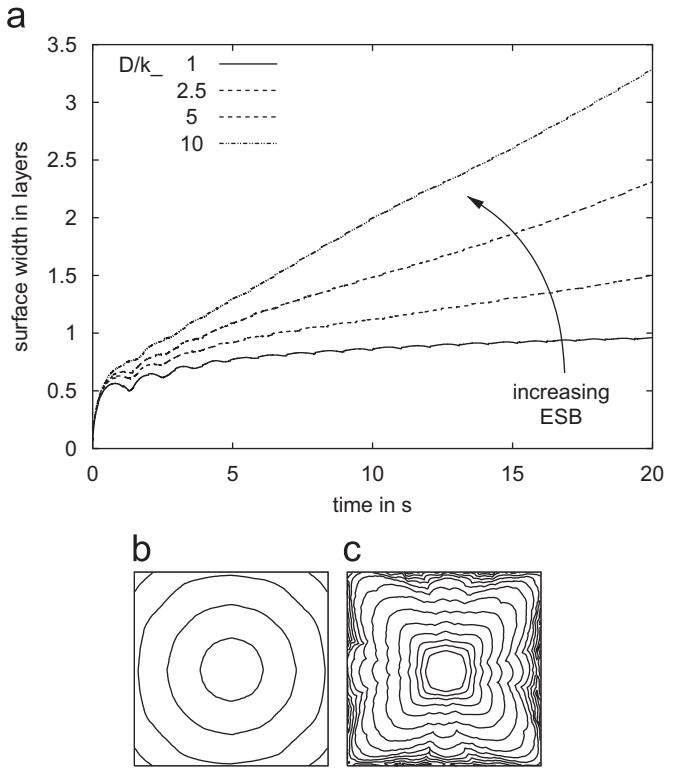

Fig. 8. (a) Surface width over time for several values of d_-. The step configuration is shown after 16 s for (b) $d_- = 1$ and (c) $d_- = 10$. Keeping the other parameters constant as before, the strength of the ESB is increasing with increasing d_-.

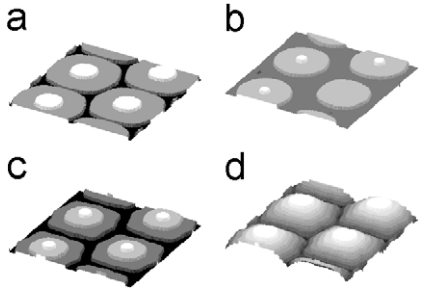

Fig. 9. Simulation of four mounds. (a) and (b) show two snapshots after 1 and 5 s of deposition without ESB. (c) and (d) show snapshots after 1 and 5 s of deposition with ESB, $d_- = 10$.

4. Conclusions

We adapted a cellular automata (CA) algorithm in order to track the steps in a Burton–Cabrera–Frank framework. The algorithm is validated for two instabilities due to the Ehrlich–Schwoebel barrier (ESB): meander instability and mound formation. The Bales–Zangwill instability is quantitatively reproduced by the numerical method. The onset of mound formation is shown qualitatively.

The equations describing adatom diffusion is solved by finite differences on the same scale as the CA. The ESB is included by kinetic boundary condition at the step. In order to treat the non-trivial boundary condition with FDs a ghost value method is described.

A new CA algorithm has been developed to track the steps during epitaxial growth. The CA provides a grid based description of the step. Thus, morphological changes and impingement of steps are easily treated. Special effort has been made to extract a smooth approximation of the step out of the CA.

The CA algorithm is by nature a local algorithm. That is, the information of the boundary is mostly stored on grid cells near the step and the step propagation is only dependent on the neighboring cells. So local effects may be modeled naturally, e.g., nucleation. The local nature of the algorithm is perfectly suited to account for short range interaction of steps, e.g., step pairing. Furthermore, the new CA algorithm is specially constructed to overcome and control the intrinsic anisotropy of the CA by rectangular EEs. The intrinsic anisotropy of the CA, which we are now able to control, is a promising feature of the CA. That is, corners of the step may be represented by the CA directly. Regularizations as needed for parametric elements, level sets or phase field are not needed [15,16]. In further studies we want to exploit the intrinsic anisotropy to model anisotropic growth laws in epitaxy. Additionally we want to combine simulations of step trains with nucleation.

Acknowledgment

This work has been partially supported by EU FP6, through NMP STRP 016447 "MagDot".

References

[1] W.K. Burton, N. Cabrera, F.C. Frank, Philos. Trans. R. Soc. London Ser. A 243 (866) (1951) 299.
[2] R.L. Schwoebel, J. Appl. Phys. 40 (1969) 614.
[3] E. Bänsch, F. Haußer, O. Lakkis, B. Li, A. Voigt, J. Comput. Phys. 194 (2004) 409.
[4] S. Chen, B. Merriman, M. Kang, R.E. Caflisch, C. Ratsch, L. Cheng, M. Gyure, R.P. Fedkiw, C. Anderson, S. Osher, J. Comput. Phys. 167 (2001) 475.
[5] Y.-M. Yu, B.-G. Liu, Phys. Rev. E 69 (2004) 021601.
[6] F. Otto, P. Penzler, A. Rätz, T. Rump, A. Voigt, Nonlinearity 17 (2004) 477.
[7] CH.-A. Gandin, M. Rappaz, Acta Mater. 45 (5) (1996) 2187.
[8] P. Politi, C. Castellano, Phys. Rev. E 66 (2002) 031605.
[9] P. Politi, C. Castellano, Phys. Rev. E 67 (2003) 075408.
[10] Iterative Methods Library (IML++) ⟨http://math.nist.gov/iml++/⟩.
[11] C. Ratsch, J. Garcia, R.E. Caflisch, Appl. Phys. Lett. 87 (2005) 141901.
[12] G.S. Bales, A. Zangwill, Phys. Rev. B 41 (1990) 5500.
[13] A. Pimpinelli, I. Elkinani, A. Karma, C. Misbah, J. Villain, J. Phys. Condens. Matter 6 (1994) 2661.
[14] J. Krug, Physica A 313 (2002) 47.
[15] F. Haußer, A. Voigt, Appl. Math. Lett. 19 (2006) 691.
[16] C.Y. Kao, S. Osher, J. Qian, J. Comput. Phys. 196 (1) (2004) 367.